








Gain-compensated cavities for the dynamic control of light-matter interactionsChristos Tserkezis ^{1,2} Christian Wolff ^{1,2} Fedor A. Shuklin ^{1,2} Francesco Todisco ^{3,1,2} Mikkel H. Eriksen ^{1,2}
P. A. D. Gonçalves ^{2,*} and N. Asger Mortensen ^{1,2,4}¹*POLIMA—Center for Polariton-driven Light–Matter Interactions,**University of Southern Denmark, Campusvej 55, DK-5230 Odense M, Denmark*²*Center for Nano Optics, University of Southern Denmark, Campusvej 55, DK-5230 Odense M, Denmark*³*CNR NANOTEC, Institute of Nanotechnology, Via Monteroni, I-73100 Lecce, Italy*⁴*Danish Institute for Advanced Study, University of Southern Denmark, Campusvej 55, DK-5230 Odense M, Denmark*

(Received 20 September 2022; accepted 3 April 2023; published 19 April 2023)

We propose an efficient approach for actively controlling the Rabi oscillations in nanophotonic emitter-cavity analogs based on the presence of an element with optical gain. Inspired by recent developments in parity-time (\mathcal{PT})-symmetry photonics, we show that nano- or microcavities where intrinsic losses are partially or fully compensated by an externally controllable amount of gain offer unique capabilities for manipulating the dynamics of extended (collective) excitonic emitter systems. In particular, we discuss how one can drastically modify the dynamics of the system, increase the overall occupation numbers, enhance the longevity of the Rabi oscillations, and even decelerate them to the point where their experimental observation becomes less challenging. Furthermore, we show that there is a specific gain value that leads to an exceptional point, where both the emitter and cavity occupation oscillate practically in phase, with occupation numbers that can significantly exceed unity. By revisiting a recently introduced Rabi-visibility measure, we provide robust guidelines for quantifying the coupling strength and achieving strong-coupling with adaptable Rabi frequency via loss compensation.

DOI: [10.1103/PhysRevA.107.043707](https://doi.org/10.1103/PhysRevA.107.043707)**I. INTRODUCTION**

The possibility to control the emission of light from natural or artificial light sources at the nanoscale has attracted considerable interest [1–7] ever since Purcell showed that the dynamics of an emitter is strongly affected by its environment [8]. The tremendous opportunities that such control enables have kept inspiring novel designs for efficient cavities, appropriately tailored depending on the emitters under consideration. Mirror cavities, the prototypical templates in cavity quantum electrodynamics [9,10], have long been employed as the most straightforward choice when considering atoms [11], while Bragg reflectors and photonic crystals constitute a natural option for artificial emitters such as quantum wells and dots [12,13]. More recently, excitons in molecular aggregates or transition-metal dichalcogenides (TMDs) [14] have been introduced as emitters with strong, collective (i.e., *effective*) dipole moments, leading to the emergence of, among others, plasmonic [15–20] and Mie-resonant [21–24] nanostructures as suitable effective cavities. What really determines the appropriateness of the cavity in all these endeavors is the linewidth of the emitter: the optical mode must be chosen to have a comparable linewidth, and the coupling strength must exceed the damping rates of the individual components

[1]. Nevertheless, in addition to this fundamental requirement, various other optical properties that might characterize the cavity can readily open new routes for the manipulation of the strong-coupling response [25–28].

A major boost in the quest for photonic templates with novel, possibly “exotic,” optical properties was recently provided by the adoption of the concept of non-Hermiticity [29]. While initially introduced in the context of nuclear physics, non-Hermitian Hamiltonians eventually found a fertile playground in photonics [30], especially after the realization that they can still have real eigenvalues, as long as they commute with the parity-time (\mathcal{PT}) operator [31]. Their appeal in photonics is due to the fact that \mathcal{PT} -symmetric potentials can be achieved by incorporating a gain element—widely available in optics since the development of lasers—that compensates the intrinsic loss of the system [32,33]. Explorations of \mathcal{PT} symmetry have often revealed surprising responses and intriguing novel designs, including unidirectional propagation [34–37] and cloaking [38,39], lasers [40–42], gyroscopes [43], nanoantennas [44], and potentially powerful sensors operating at the exceptional point (EP) [45–49], i.e., the condition under which the eigenstates of the Hamiltonian coalesce and the corresponding eigenvalues are equal.

Inspired by these developments and the richness of optical phenomena that can benefit from loss-gain combinations, we explore here the possibility of designing optical cavities in which the emergence and time evolution of strong coupling can be dynamically controlled through the externally provided gain. We theoretically show that by increasing the amount

*Present address: ICFO—Institut de Ciències Fotòniques, Barcelona Institute of Science and Technology, E-08860 Castelldefels (Barcelona), Spain.

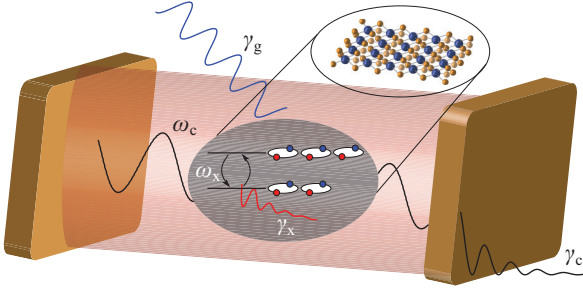


FIG. 1. Schematic of the explored strong-coupling cavities: a typical cavity formed by two mirrors, supporting a single optical mode with frequency ω_c and damping rate γ_c . Gain is provided to it externally, at a rate γ_g . A QE system with a composite-bosonic character, formed by collective excitonic resonances in extended systems such as TMDs (as shown in the zoom-in sketch), with transition frequency ω_x and damping rate γ_x , is placed between the mirrors and couples to the cavity mode with coupling constant g .

of gain it is possible to drive the exciton-cavity system to increase the number of Rabi oscillations that can be measured before damping prevails and the system completely loses its coherence. We revisit a recently introduced visibility measure [22] and provide a detailed gain-coupling map that quantifies the different coupling regimes; based on this, one can manipulate the dynamics of the system and accelerate or decelerate the Rabi oscillations to render their period more easily resolvable in experiments. Backtracking the visibility map, one can then extrapolate to infer the properties of the coupled system in the absence of gain. Finally, we show that by further increasing the gain along specific paths, one can reach an EP, where the dynamics of the system is completely altered, and the occupations of both emitter-cavity polariton modes significantly exceed unity and oscillate nearly in phase. This set of different behaviors indicates that inclusion of gain can open new ways for tailoring the dynamics of coupled emitter-cavity architectures, with both fundamental understanding and practical applications in mind. Analogous phenomena have already been observed for optical [50] and magnonic [51] waveguides operating at the EP, but here, we generalize the treatment for any kind of collective polaritonic system. We anticipate that related experiments can readily benefit from the techniques developed in the context of \mathcal{PT} symmetry [30].

II. HAMILTONIAN DESCRIPTION

We focus on extended, collective excitonic states like those encountered in J aggregates, individual organic molecules, and TMDs coupled to a (possibly open) micro- or nanocavity such as a distributed Bragg reflector, a metallic nanoparticle, or simply a pair of mirrors, as suggested by the schematic in Fig. 1. Expressing all the interactions in terms of the actual Hamiltonian of the system thus becomes cumbersome since one should include interaction among excitons [52], together with the appropriate Lindblad operators to account for both loss and gain [53]. We therefore restrict ourselves to a toy-model description that essentially follows classical coupled-mode theory [54]. We thus formulate the coupling problem in terms of a (semiclassical) interaction Hamiltonian.

To make the description as widely applicable as possible, we consider a generic excitonic material, modeled by a simple Lorentzian permittivity, with transition frequency ω_x and intrinsic linewidth γ_x , coupled to a cavity with resonance frequency ω_c and damping rate γ_c . Within this description, the dynamics is then governed by the Schrödinger-like equation

$$\begin{pmatrix} \omega_c - i\frac{\gamma_c}{2} + i\frac{\gamma_g}{2} & g \\ g & \omega_x - i\frac{\gamma_x}{2} \end{pmatrix} \begin{pmatrix} a(t) \\ b(t) \end{pmatrix} = i\frac{\partial}{\partial t} \begin{pmatrix} a(t) \\ b(t) \end{pmatrix}, \quad (1)$$

where g is the coupling constant and γ_g is a possible gain rate added to the cavity. What we aim to explore here is whether, and to what extent, the latter can be used as a means for loss compensation that would eventually enhance the visibility of Rabi-like oscillations in the strong-coupling regime. A schematic of a typical cavity composed of two mirrors is shown in Fig. 1. A quantum emitter (QE), sketched in the figure as a generic bosonic [55] system that could correspond to the TMD shown in the zoom, characterized by an overall effective emitter dipole moment, is placed between the two resonators and couples to a single cavity mode when the detuning $\omega_x - \omega_c$ is sufficiently small. In addition to the usual characteristics of such cavities, as encountered in quantum optics, a gain element is also included here (Fig. 1), e.g., by the inclusion of an active material that does not interact with the QE or via asymmetric pumping [61]. While, for our purposes, it is sufficient to accept that some gain mechanism can exist, it should be acknowledged that precise control of the gain rate is, in practice, a challenging task which requires carefully designed experiments appropriately adapted to the gain medium of choice, which, ideally, should have a linewidth comparable to those of the emitter and the cavity. Possibilities include electrochemical doping for quantum dots [62] and TMDs [63], spatial modulation [64], state-resolved optical pumping [65], and host-guest chemistry [66].

To describe the dynamics of the coupled system, we first assume, for simplicity, a perfect frequency alignment between the cavity and the exciton; this zero detuning is what most experiments try to achieve to better evaluate the coupling properties [67–69]. Without loss of generality, we can then measure all energies with respect to this frequency, i.e., set $\omega_c = \omega_x = 0$. We focus on time-harmonic solutions of the form $e^{-i\omega t}$ and introduce frequencies and times normalized to the linewidth of the exciton system: $\Omega \equiv 2\omega/\gamma_x$ and $\tau \equiv \gamma_x t/2$. Likewise, we introduce the normalized coupling $G \equiv 2g/\gamma_x$ and the normalized damping rate $\Gamma \equiv (\gamma_g - \gamma_c)/\gamma_x$. In what follows, we will explore the dynamics as Γ varies from -1 (e.g., a cavity in the absence of gain with a linewidth matching that of the QE) to $+1$ (i.e., where the gain not only compensates the cavity losses but also exactly balances the broadening of the exciton), thus producing long-lived Rabi-like oscillations. The time-harmonic solutions are now governed by the dimensionless eigenvalue problem

$$\begin{pmatrix} i\Gamma & G \\ G & -i \end{pmatrix} \begin{pmatrix} a(\tau) \\ b(\tau) \end{pmatrix}_{\pm} = \Omega_{\pm} \begin{pmatrix} a(\tau) \\ b(\tau) \end{pmatrix}_{\pm}, \quad (2)$$

whose diagonalization yields the eigenfrequencies

$$\Omega_{\pm} = -\frac{i}{2}(1 - \Gamma) \pm \frac{1}{2}\sqrt{4G^2 - (1 + \Gamma)^2}. \quad (3)$$

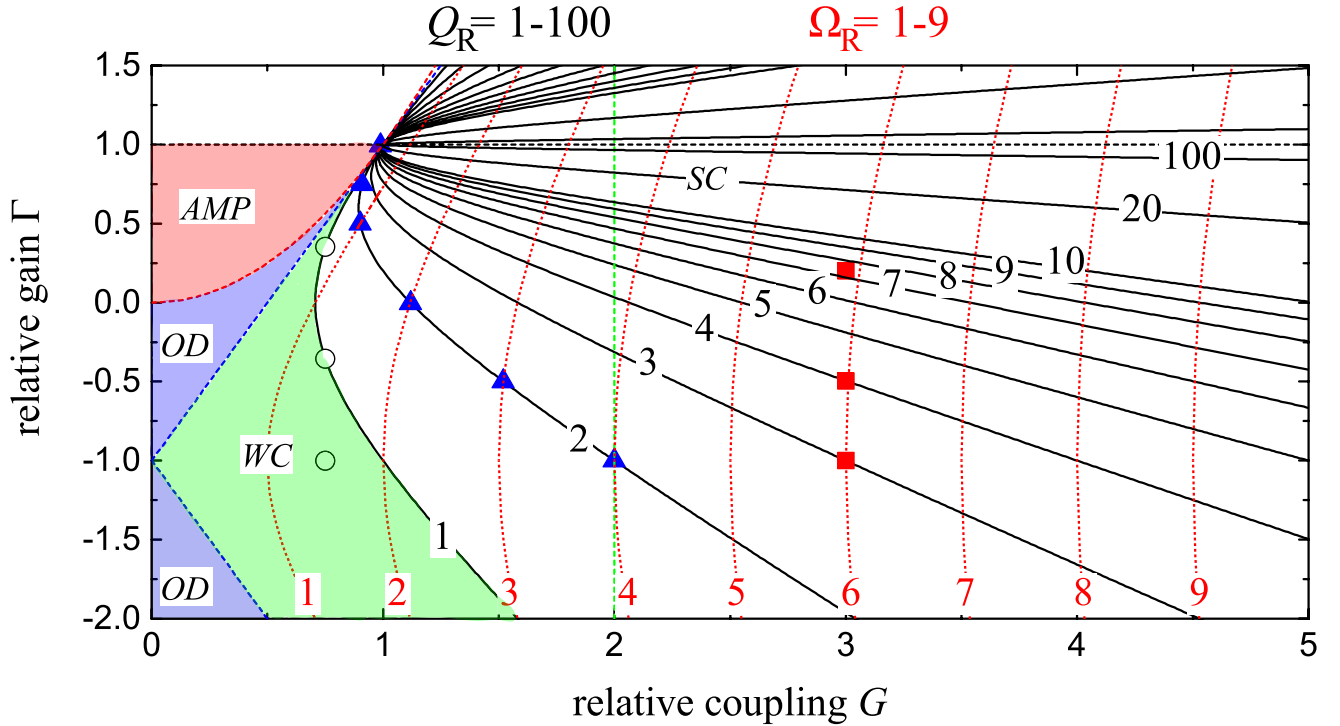


FIG. 2. Rabi-oscillation visibility quality factor Q_R as a function of the relative gain Γ and relative coupling G . Partial loss compensation occurs whenever $\Gamma > -1$, with $\Gamma = 0$ corresponding to the case of a gain-balanced cavity ($\gamma_g = \gamma_c$) and $\Gamma = 1$ corresponding to the case of fully gain-compensated exciton-cavity system (i.e., $\gamma_g = \gamma_c + \gamma_x$). When $2G = |\Gamma + 1|$ (blue dashed lines), the two solutions of Eq. (2) coalesce and give rise to EPs; the one at $\Gamma = G = 1$ is particularly important, and all Q_R isocontours cross it. The blue shaded region (OD) is characterized by critical damping, while the red shaded region (AMP) exhibits amplification. The weak-coupling regime (WC, green shaded region) and the strong-coupling regime (SC, white region) are separated by the $Q_R = 1$ curve. Black curves indicate isocontours corresponding to different Q_R , as indicated by the labels in black; red dotted curves indicate isofrequency contours (constant Ω_R), with the (normalized) values of the frequencies labeled in red. Open circles, blue triangles, and red squares correspond to specific G and Γ combinations discussed in the text.

In these dimensionless parameters, the Rabi-like frequency $\Omega_R = \Omega_+ - \Omega_-$ becomes

$$\Omega_R = \sqrt{4G^2 - (1 + \Gamma)^2}, \quad (4)$$

which is a generalization of the familiar result $\Omega_R = 2G$ (for only $\Gamma = -1$). However, the introduction of gain also opens the possibility for an EP, the condition being $\Gamma = \pm 2G - 1$ (which corresponds to $\gamma_g = \pm 4g + \gamma_c - \gamma_x$). This condition dictates the transition between an oscillating system and an overdamped (OD) system, shown by the blue dashed line in the coupling map in Fig. 2. When this is fulfilled, the square root vanishes, leading to vanishing splitting $\Omega_R = 0$. In fact, the fulfillment of the aforementioned condition, i.e., $2G = |\Gamma + 1|$, corresponds to a manifold of exceptional points, where the \mathcal{PT} symmetry leads to coalescent eigenstates with entirely real eigenvalues $\Omega_{\pm} = 0$. Hereafter, in our analysis we focus on one such EP, namely, that defined by $G = \Gamma = 1$, which is henceforth denoted EP* and corresponds to a scenario where the gain exactly balances the combined losses associated with the linewidths of the cavity and emitter. As we shall see below, this point has intriguing consequences for the dynamics of the ensuing light-matter interaction. Finally, based on Eq. (3), we can define the amplification region through $\text{Im}\Omega_{\pm} > 0$. One such amplification region, for which $\Gamma < 1$ and $(1 + \Gamma)^2 > 4G^2$, is highlighted in light red in the

top left corner of Fig. 2; nevertheless, it still lies in the OD regime.

III. VISIBILITY MEASURE

Before considering specific values of the normalized gain and exploring how they affect the QE-cavity coupling, it is useful to introduce a visibility measure for the Rabi oscillations in terms of the quality factor $Q_R = \text{Re}[\Omega_- - \Omega_+] / \text{Im}[\Omega_- + \Omega_+]$. Such quality factors have already been introduced in the literature to deal with gainless strongly coupled systems [22,70], but here, we generalize their applicability to the case of cavities with gain. From Eq. (3), we straightforwardly obtain (while also assuming $2G \geq |1 + \Gamma|$)

$$Q_R = \frac{\sqrt{4G^2 - (1 + \Gamma)^2}}{1 - \Gamma} = \frac{\sqrt{(4g)^2 - (\gamma_x + \gamma_g - \gamma_c)^2}}{\gamma_x - \gamma_g + \gamma_c}. \quad (5)$$

In the spirit of ring-down spectroscopy [71], this quality factor quantifies the number of “round trips,” i.e., the number of resolvable oscillations of light between the cavity and the emitter. In passing, we emphasize how the linewidths are naturally added up in accordance with Matthiessen’s rule for the addition of scattering rates [72]. Introduction of this measure for the visibility of Rabi-like oscillations allows us to

TABLE I. Strong-coupling experiments sorted by increasing Q_R . The similarity sign (\sim) is used when the data listed here are not mentioned explicitly by the authors of the corresponding reference but are roughly estimated in this paper. In all of these experiments, $\gamma_g = 0$, and thus, $\Gamma = -\gamma_c/\gamma_x$.

| Ref. | Cavity | Quantum emitter | g (meV) | γ_x (meV) | γ_c (meV) | G | Γ | Q_R |
|------|-----------------------------|-------------------------------|----------------------|-----------------------|-----------------------|-------------------|-----------------------|-------|
| [73] | Localized plasmon resonance | TMD exciton | 45 | 50 | 110 | 1.80 | -2.2 | 1.1 |
| [69] | Localized plasmon resonance | TMD exciton | 64 | 28 | 170 | 4.57 | -6.07 | 1.1 |
| [17] | Localized plasmon resonance | J -aggregate exciton | 81 | 100 | 109 | 1.62 | -1.09 | 1.6 |
| [74] | Bragg mirror | Halide perovskite | 48 | 90 | 25 | 1.06 | -0.28 | 1.6 |
| [68] | Plasmon-lattice resonance | J -aggregate exciton | 137.5 | 80 | 200 | 3.44 | -2.50 | 1.9 |
| [75] | Semiconductor microcavity | Organic semiconductor exciton | 80 | 90 | 22 | 1.77 | -0.24 | 2.8 |
| [19] | Localized plasmon resonance | Dye-molecule exciton | 152.5 | 85 | 122 | 3.59 | -1.44 | 2.9 |
| [15] | Surface-plasmon resonance | J -aggregate exciton | 90 | 50 | 70 | 3.6 | -1.4 | 3.0 |
| [67] | Localized plasmon resonance | J -aggregate exciton | 200 | 100 | 150 | 4 | -1.5 | 3.2 |
| [16] | Surface-plasmon resonance | J -aggregate exciton | 125 | ~ 0.66 | ~ 140 | 380 | -213 | 3.4 |
| [76] | Plasmon-lattice resonance | J -aggregate exciton | ~ 350 | ~ 20 | ~ 200 | 37.5 | -10 | 4 |
| [77] | Terahertz metamaterial | 2DEG cyclotron transition | ~ 4.1 | ~ 0.41 | ~ 0.12 | 20 | -0.29 | 31 |
| [78] | Semiconductor microcavity | 2DEG intersubband transition | 7 | 5 | 15 | 5.6 | -3 | 45 |
| [79] | Superconducting microcavity | Atomic beam | 2.9×10^{-8} | 2.1×10^{-9} | 1.7×10^{-12} | 28 | -8.0×10^{-4} | 56 |
| [80] | Superconducting microcavity | Circular Rydberg atoms | 1.0×10^{-7} | 2.1×10^{-11} | 3.0×10^{-9} | 1.0×10^4 | -145 | 137 |
| [81] | Mirror cavity | Bose-Einstein condensate | 1.3×10^{-3} | 1.2×10^{-5} | 5.4×10^{-6} | 213 | -0.4 | 298 |

rigorously discuss the weak-coupling (WC) versus strong-coupling regimes. Strong coupling occurs for $Q_R > 1$, corresponding to $G > \sqrt{(1 + \Gamma^2)}/2$ (white region in Fig. 2), which is perfectly in line with the more common definition that the splitting should exceed the linewidth [1]. On the other hand, for $Q_R < 1$ the dynamics will have all the characteristics associated with the WC regime (light-green area in the left part of Fig. 2); as Q_R approaches zero, the system enters either an OD regime (blue triangular regions on the left in Fig. 2) or the regime with net amplification, depending on the relative gain. This is summarized in the parameter phase space of Fig. 2, which provides a direct and intuitive guide for manipulating the coupling via application of gain. The black curves correspond to isocontours of Q_R (values given with numbers in black), while the dotted red curves are isofrequency contours for the Ω_R values given at the bottom of each curve in red.

To evaluate the usefulness of Q_R , it is insightful to examine how state-of-the-art experiments from the literature classify according to this measure. Such a comparison is done in Table I for a variety of QEs and cavities, most of which employ surface plasmons or localized plasmon resonances in nanoparticles as cavities, except for a one-dimensional photonic crystal in Ref. [75] and quantum optical systems in Refs. [79–81]. None of the experiments listed in Table I used gain, meaning that the listed Γ corresponds to the normalized damping rate of the cavity alone (i.e., $\Gamma = -\gamma_c/\gamma_x$). Using this Γ together with γ_x , one can then straightforwardly estimate whether the usual strong-coupling criterion

$$\Omega_R > \frac{\gamma_x + \gamma_c}{2} \quad (6)$$

holds. This criterion is not normalized to any intrinsic property of the system, and it is therefore difficult to use it to compare different types of strong-coupling configurations, whereas Q_R is properly normalized and can then be applied

to a wide variety of systems. Hence, the predictions of Eq. (6) do not strictly follow the computed Q_R appearing in Table I.

Inspecting Table I, it appears that the highest Q_R (≥ 3) for nanophotonic systems are still achieved by architectures employing J aggregates coupled to plasmonic systems [15,16,67]. This excellent performance is related to the high out-of-plane dipole moments of the J -aggregated molecules and the intense near fields provided by the plasmonic cavities. TMD-based systems, on the other hand, seem to be the most poorly performing at the moment. This has to do both with the fact that such activities have only recently emerged, leaving considerable room for improvement, and with the fact that the effective dipole moment associated with excitons in these two-dimensional (2D) materials lie predominantly in plane, making the coupling with any out-of-plane cavity mode less efficient. In this respect, 2D halide perovskites, with their dipole moments oriented out of plane [82], might provide an efficient alternative for 2D polaritonics in the future [74,83]. Similarly, high-quality factors are also obtained for emitters based on 2D electron gases (2DEGs) in the case of either intersubband transitions [78] or cyclotron transitions [77]. Nevertheless, despite the recent advances in nanophotonics, the highest performance in terms of Q_R lies still in the quantum-optical domain, involving ultrahigh-finesse (e.g., superconducting) cavities or Rydberg atoms. This is to be expected since in those platforms the linewidths of both cavities and QEs can be very small, and all the experiments in Refs. [79–81] have been carried out at cryogenic temperatures. Of course, the requirement for such conditions and the costs that accompany them were one of the main motivations for shifting attention towards room-temperature nanophotonics in the first place. One should thus always keep in mind the specific purpose that any new strong-coupling configuration would serve and find the best balance between performance and cost. In passing,

we should also mention that the values of relative Γ that we obtain by analyzing the data reported in Refs. [79–81] are rather unconventional and unexpected (according to our previous definition, values below -1 are expected for systems that are not externally pumped, while values between -1 and 0 correspond to the presence of some kind of gain); these experiments typically involved single atoms and/or photons, and adoption of our Q_R measure should be done more judiciously.

IV. TIME EVOLUTION

In order to further substantiate the usefulness of the above visibility measure—also in the time domain—and to clearly display that the parameter space in Fig. 2 indeed quantifies the weak- versus strong-coupling regimes and the visibility of Rabi oscillations in the latter case, we next consider the time evolution of the cavity and emitter occupation numbers (herein not normalized due to the semiclassical incorporation of gain). Starting with Eq. (1), the time evolution can be solved straightforwardly (see the Appendix). For the initial conditions of an empty cavity and an excited emitter, i.e., $a(0) = 0$ and $b(0) = 1$, we find

$$|a(\tau)|^2 = \frac{4G^2}{\Omega_R^2} e^{-\frac{\Omega_R \tau}{Q_R}} \sin^2\left(\frac{1}{2}\Omega_R \tau\right) \\ = \frac{2G^2}{\Omega_R^2} e^{-\frac{\Omega_R \tau}{Q_R}} [1 - \cos(\Omega_R \tau)], \quad (7a)$$

$$|b(\tau)|^2 = e^{-\frac{\Omega_R \tau}{Q_R}} \left[\cos(\Omega_R \tau) - \frac{(1 + \Gamma)}{\Omega_R} \sin(\Omega_R \tau) \right] + |a(\tau)|^2. \quad (7b)$$

From these exact analytic expressions, it is unambiguously clear that the occupation numbers oscillate with a period governed solely by Ω_R , while only a number of Q_R oscillations are visible, as a consequence of the overall exponential decay factor $e^{-\frac{\Omega_R \tau}{Q_R}}$. Thus, our introduction of Q_R is more than a convenient parametrization—it is the unique measure that emerges from a systematic dimensionless formulation of the problem. We emphasize that, while, initially, $|a(0)|^2 + |b(0)|^2 = 1$, there is no such conservation after a finite time. This is always anticipated in realistic systems due to the dispersive and lossy nature of the cavity and the QE, but in our case, because of the presence of gain, the sum of the two occupation numbers can and, indeed, does exceed unity. In what follows we will explore the dynamics of Eqs. (7) for different limits of the parameter space depicted in Fig. 2 and discuss how the presence of gain can drastically affect the dynamics of the problem.

A. Weak-coupling dynamics

In the weak-coupling regime, with $Q_R \ll 1$, the general solution of Eq. (7) can be significantly simplified. This is the Weisskopf-Wigner regime [84], where the cavity exhibits an initial quadratic rise,

$$|a(\tau)|^2 \approx (G\tau)^2 e^{-\frac{\Omega_R \tau}{Q_R}}, \quad (8a)$$

where G naturally determines the rate of growth, while the accompanying initial dynamics of the QE is characterized by

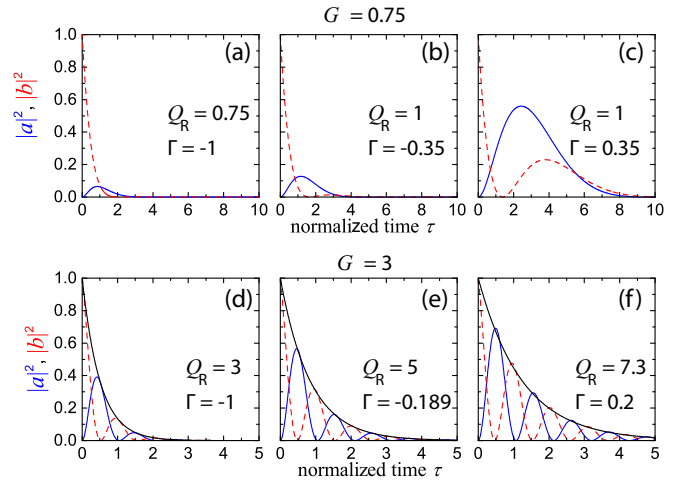


FIG. 3. Top: dynamics of the occupation numbers $|b(\tau)|^2$ (red dashed curves) and $|a(\tau)|^2$ (blue solid curves), with initial conditions $|b(0)|^2 = 1$ and $|a(0)|^2 = 0$, for three cases with $G = 0.75$ (weak-coupling regime) and (a) $\Gamma = -1.0$, (b) $\Gamma = -\sqrt{2}/4$, and (c) $\Gamma = \sqrt{2}/4$ (see open circles in Fig. 2). Bottom: similar dynamics for the strong-coupling regime with $G = 3$ and (d) $\Gamma = -1$, (e) $\Gamma = -0.189$, and (f) $\Gamma = 0.2$ (see red squares in Fig. 2). Black curves in the bottom three panels show the exponential decay envelope of Eqs. (9).

an exponential decay,

$$|b(\tau)|^2 \approx e^{-\frac{\Omega_R \tau}{Q_R}} = e^{-(1-\Gamma)\tau}. \quad (8b)$$

In Figs. 3(a)–3(c) we show this dynamics for three values of Γ along the $G = 0.75$ line in Fig. 2 (open circles). In Fig. 3(a), gain is completely absent ($\Gamma = -1$), and the system is entirely characterized by its intrinsic loss, leading to the anticipated exponential decay. Figure 3(b) corresponds to $\Gamma = -\sqrt{2}/4 \simeq -0.35$, which, according to Eq. (5) translates into the first of the two points with $Q_R = 1$, the one still dominated by loss (i.e., with $\Gamma < 0$). The emergence of the first oscillation in $|b(\tau)|^2$ is, indeed, (hardly) discernible in the red dashed curve. Finally, Fig. 3(c) corresponds to $\Gamma = \sqrt{2}/4 \simeq 0.35$, i.e., the second condition for which $Q_R = 1$ in Fig. 2; the external gain has now started driving the system, so that a full oscillation in $|b(\tau)|^2$ can be observed before its eventual decay. According to Fig. 2, it is feasible to drive the system into the strong-coupling regime, just between these two points (before the $Q_R = 1$ curve bends back again for higher gain). On the other hand, keeping G constant, say, at 0.75 , and moving vertically in Fig. 2 provide a recipe for tailoring the Purcell factor in the weak-coupling regime. The Purcell factor expresses the acceleration of the spontaneous emission rate in a cavity; the rate itself is essentially proportional to the square of the coupling strength and inversely proportional to the damping of the cavity [85]. Consequently, for a fixed G , Fig. 2 suggests that the spontaneous emission rate increases, leading to a larger Purcell factor. Finally, it is also important to observe that the period of the oscillations has increased (in accordance with the shape of the isofrequency contours in this region) and the two populations are more in phase; this will become relevant again in the subsequent analysis.

B. Strong-coupling dynamics

Deep into the strong-coupling regime, where $G \gg 1$, Eqs. (7) simplify to

$$|a(\tau)|^2 \simeq e^{-\frac{\Omega_R \tau}{Q_R}} \sin^2\left(\frac{1}{2}\Omega_R \tau\right), \quad (9a)$$

$$|b(\tau)|^2 \simeq e^{-\frac{\Omega_R \tau}{Q_R}} \cos^2\left(\frac{1}{2}\Omega_R \tau\right). \quad (9b)$$

Here, we clearly see how the two occupation numbers evolve fully out of phase; that is, energy bounces back and forth between the excitonic component and the cavity while, of course, still being exponentially damped over time. In turn, these expressions imply that $|a(\tau)|^2 + |b(\tau)|^2 \simeq e^{-\frac{\Omega_R \tau}{Q_R}}$. This is the common strong-coupling dynamics [84]. Here, it is immediately evident that Q_R quantifies the number of oscillations before reaching full relaxation: what the addition of gain achieves is to increase the number of oscillations that are visible before complete decay. Corresponding results are shown in Figs. 3(d)–3(f) for $G = 3$ (red squares in Fig. 2). When the system is not compensated [$\Gamma = -1$; Fig. 3(d)], three oscillations are observable in the dynamics (the third is only just visible). By increasing the amount of gain provided to the system, one can increase the longevity of the Rabi oscillations and move vertically in the map of Fig. 2 (red squares), leading to more oscillations (still dominated by the same Rabi frequency, unlike in the previous case, as one can anticipate by observing the corresponding isofrequency contour, which is nearly vertical) that can be observed. The anticipated exponential decay is demonstrated in all three cases by the black curves.

C. Coalescing dynamics

A less explored special case that becomes relevant only in the kind of cavities with gain that we study here concerns the dynamics in the vicinity of an EP associated with \mathcal{PT} symmetry. Looking at Eqs. (7), we notice that, while $|a(\tau)|^2 \propto \Omega_R^{-2}$, the $|b(\tau)|^2$ part contains terms scaling as Ω_R^0 , Ω_R^{-1} , and Ω_R^{-2} . Approaching EP* (i.e., the EP for which $G = \Gamma = 1$), where $\Omega_R \rightarrow 0$, the Ω_R^{-2} contribution dominates, and consequently, $|b(\tau)|^2 \rightarrow |a(\tau)|^2$. This implies an intriguing in-phase time evolution of the occupation numbers, which is a remarkable consequence of \mathcal{PT} symmetry and the coalescing eigenstates at EPs.

To see how the dynamics changes as EP* is approached, we follow in Fig. 4 the $Q_R = 2$ curve for increasing Γ (see blue triangles in Fig. 2). In Figs. 4(a)–4(c), the composite cavity is still lossy overall. In all cases, two oscillations are observed (the second is one barely observed), as expected, but their period increases as the provided gain increases, in accordance with the behavior of the weakly coupled system in Fig. 3. This behavior could be immediately anticipated based on the isofrequency contours in Fig. 2: following the $Q_R = 2$ line means crossing several of the dotted red contours, with the frequency decreasing as gain increases. In Figs. 4(d)–4(f) the system is practically externally driven by the gain. As the gain increases and EP* is approached, the Rabi oscillations decelerate further, both populations increase beyond the initial condition of unity, and their phase difference becomes ever smaller. Near EP* (which cannot be reached exactly, so we can approach it only adiabatically), both populations oscillate practically in phase and coincide in their maximum values;

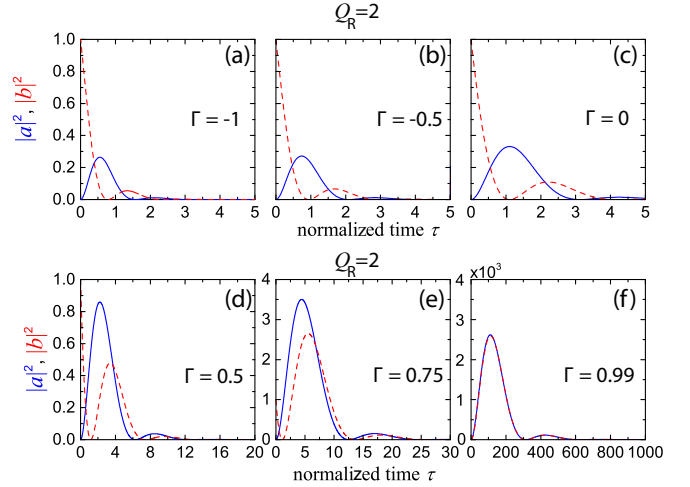


FIG. 4. Dynamics of the occupation numbers $|b(\tau)|^2$ (red dashed curve) and $|a(\tau)|^2$ (blue solid curve), with initial conditions $|b(0)|^2 = 1$ and $|a(0)|^2 = 0$, for six cases on the $Q_R = 2$ contour with (a) $\Gamma = -1$, (b) $\Gamma = -0.5$, (c) $\Gamma = 0$, (d) $\Gamma = 0.5$, (e) $\Gamma = 0.75$, and (f) $\Gamma = 0.99$; see blue triangles in Fig. 2.

the system is driven externally and has approached the net amplification regime.

V. RABI-OSCILLATION RETRIEVAL

The gain-induced changes in the dynamics discussed above suggest that one might be able to use gain to characterize the time evolution of the system even if its initial Rabi oscillations are too fast to be experimentally traceable (e.g., as in typical plasmon-exciton coupling systems where Ω_R can be substantial, even though the corresponding Q_R are often modest due to the sizable γ_c). To this end, we plot in Fig. 5 the period of the oscillations as a function of the externally provided gain for couplings ranging from $G = 1$ to 2.5. As the relative gain increases, one moves vertically along Fig. 2, meaning that Q_R is expected to increase rapidly, especially for relatively small G , for which the isofrequency contours are more curved. At the same time, following the previous discussion, the period of the oscillations is also expected to increase since it is just $T = 2\pi/\Omega_R$, with Ω_R given by Eq. (4). This is, indeed, shown in Fig. 5(a) for four cases of relatively small (but larger than unity) G . One immediately observes that the weaker the coupling is, the more it can be affected by the exertion of gain, again in agreement with the isofrequency contours in Fig. 2. Three typical examples of the dynamics are shown in Figs. 5(b)–5(d) for $G = 2$ (along the vertical green dashed line in the middle of Fig. 2), where the relative gain increases from $\Gamma = -1.0$ (no gain) to $\Gamma = 0$ (fully compensated cavity) and $\Gamma = 0.99$ (gain-dominated cavity). As discussed above, not only does the number of observable Rabi oscillations increase, but they also decelerate (i.e., their period increases), while, eventually, the populations exceed unity, as expected.

What one can immediately observe in the dynamics of Fig. 5(a) is that the period of the oscillations follows an inverse-square dependence on Γ , as expected from Eq. (4) and as one can retrieve by calculating specific examples of dynamics. This suggests a way to deduce the period of Rabi oscillations in ultrafast QE-cavity systems, where the oscillations,

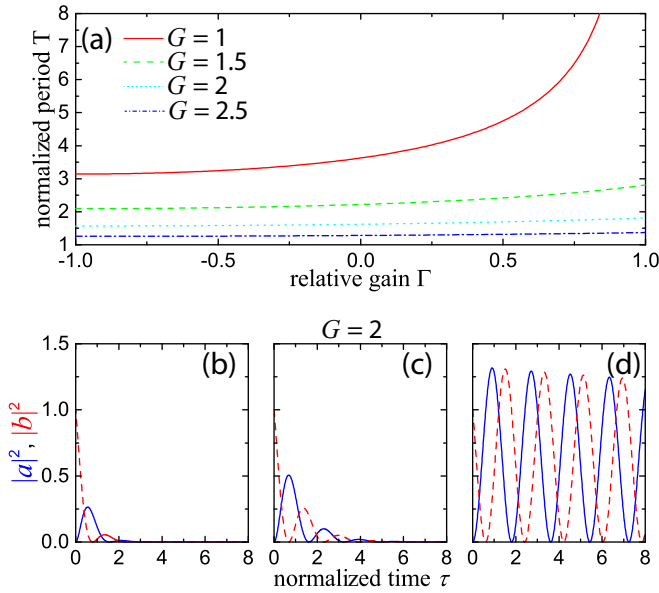


FIG. 5. (a) Normalized period of the Rabi oscillations for a QE-cavity system with G equal to 1 (solid red line), 1.5 (dashed green line), 2 (dotted light-blue line), and 2.5 (dash-dotted blue line) as a function of the externally provided normalized gain Γ . The period clearly follows an inverse square-root law, in agreement with Eq. (4). Time dynamics of the occupation numbers $|b(\tau)|^2$ (red dashed curves) and $|a(\tau)|^2$ (blue solid curves), with initial conditions $|b(0)|^2 = 1$ and $|a(0)|^2 = 0$, for $G = 2$ and (b) $\Gamma = -1$, (c) $\Gamma = 0$, and (d) $\Gamma = 0.99$.

with periods of a few femtoseconds, cannot be resolved with current instruments. But in a loss-compensated cavity, where the gain is externally controlled, one can increase the period of the oscillations to the point where the instrument resolution allows clear observation of the dynamics and then extrapolate to the expected value in the absence of gain. Gain-dominated cavities thus provide the means to not only manipulate the dynamics of the QE-cavity system but also potentially characterize it through gradual modification of the provided gain.

VI. CONCLUSION

We have analyzed the dynamics of QEs coupled to optical cavities that can be controlled via externally provided gain. Based on a general Rabi-visibility criterion that quantifies the number of oscillations that one should expect to observe in an experiment, we established three different coupling regimes, namely, weak, strong, and coalescing. We showed that the provided gain affects these three regimes differently. When the coupling strength G is large, the dynamics (particularly the period of Rabi oscillations) is not considerably affected by gain, and only the populations of the ground and excited states change, being allowed to exceed unity. On the other hand, for weak and intermediate coupling strengths, externally pumping the system eventually governs the dynamics, and the period of the Rabi oscillations increases, suggesting that one could use gain to resolve ultrafast dynamics by controllably and reversibly accelerating and decelerating the oscillations. Finally, in the coalescing regime, near the EP of the resulting \mathcal{PT} -symmetric cavity, all system dynamics is completely

governed by gain, both populations oscillate nearly in phase, and they are allowed to dramatically exceed unity. Such dynamics opens up new possibilities for the design of dynamically controlled cavities for strong-coupling realizations.

ACKNOWLEDGMENTS

We thank P. Edderkop for assistance with preparation of the graphs and the web design. C.W. and F.T. acknowledge funding from MULTIPLY fellowships under the Marie Skłodowska-Curie COFUND Action (Grant Agreement No. 713694). M.H.E. acknowledges funding from Independent Research Fund Denmark (Grant No. 0165-00051B). N.A.M. is supported by VILLUM Fonden (Grant No. 16498). The Center for Polariton-driven Light-Matter Interactions (POLIMA) is sponsored by the Danish National Research Foundation (Project No. DNRF165).

APPENDIX: DETAILS ON TIME EVOLUTION

The dynamics of the coupled QE-cavity system are governed by the linear system typified by Eq. (1). Under the conditions considered in the main text (i.e., $\omega_c = \omega_x = 0$) and using the dimensionless quantities introduced there, we have

$$\frac{\partial}{\partial \tau} \begin{pmatrix} a(\tau) \\ b(\tau) \end{pmatrix} = \begin{pmatrix} \Gamma & -iG \\ -iG & -1 \end{pmatrix} \begin{pmatrix} a(\tau) \\ b(\tau) \end{pmatrix}, \quad (\text{A1a})$$

which we write compactly as

$$\dot{\mathbf{x}}(\tau) = \mathbf{A} \mathbf{x}(\tau). \quad (\text{A1b})$$

The determination of the time evolution of the state vector $\mathbf{x}(\tau)$ can be straightforwardly calculated once we are in possession of the eigenvalues λ_{\pm} and eigenvectors \mathbf{v}_{\pm} of \mathbf{A} , which read

$$\lambda_{\pm} = \frac{\Gamma - 1}{2} \pm \frac{1}{2} \sqrt{(\Gamma + 1)^2 - 4G^2} = i\Omega_{\pm} \quad (\text{A2a})$$

and

$$\mathbf{v}_{\pm} = \mathcal{N}_{\pm} \left(i \frac{\Gamma + 1 \pm \sqrt{(\Gamma + 1)^2 - 4G^2}}{2G}, 1 \right)^T, \quad (\text{A2b})$$

respectively; here, \mathcal{N}_{\pm} are normalization constants.

With the eigenvalues and eigenvectors of \mathbf{A} [see Eqs. (A1) and (A2)], the time evolution of the system follows from

$$\mathbf{x}(\tau) \equiv \begin{pmatrix} a(\tau) \\ b(\tau) \end{pmatrix} = C_1 e^{\lambda_- \tau} \mathbf{v}_- + C_2 e^{\lambda_+ \tau} \mathbf{v}_+, \quad (\text{A3})$$

that is,

$$a(\tau) = C_1 e^{\lambda_- \tau} \mathcal{N}_- \left(i \frac{\Gamma + 1 - \eta}{2G} \right) + C_2 e^{\lambda_+ \tau} \mathcal{N}_+ \left(i \frac{\Gamma + 1 + \eta}{2G} \right), \quad (\text{A4a})$$

$$b(\tau) = C_1 e^{\lambda_- \tau} \mathcal{N}_- + C_2 e^{\lambda_+ \tau} \mathcal{N}_+, \quad (\text{A4b})$$

where we have introduced $\eta = \sqrt{(\Gamma + 1)^2 - 4G^2}$ for shorthand notation. The constants $C_{1,2}$ are determined by the initial conditions; hereafter, we assume that the emitter-cavity system is initially in the state $\mathbf{x}_0 \equiv \mathbf{x}(\tau_0 = 0) = (a(0), b(0))^T =$

$(0, 1)^T$, corresponding to an empty cavity, and that all the population is in the emitter. The choice of these initial conditions implies that

$$C_1 = \frac{\Gamma + 1 + \eta}{2\eta\mathcal{N}_-}, \quad C_2 = -\frac{\Gamma + 1 - \eta}{2\eta\mathcal{N}_+}. \quad (\text{A5})$$

Then, substituting Eqs. (A5) into Eqs. (A4) yields

$$a(\tau) = \frac{iG}{\eta} [e^{\lambda-\tau} - e^{\lambda+\tau}], \quad (\text{A6a})$$

$$b(\tau) = \frac{\Gamma + 1}{2\eta} [e^{\lambda-\tau} - e^{\lambda+\tau}] + \frac{1}{2} [e^{\lambda-\tau} + e^{\lambda+\tau}]. \quad (\text{A6b})$$

Moreover, noting that $\lambda_{\pm} = i\Omega_{\pm}$, $\eta = i\Omega_R$, and $1 - \Gamma = \Omega_R/Q_R$, Eqs. (A6) can be written as

$$a(\tau) = -\frac{2iG}{\Omega_R} \sin\left(\frac{\Omega_R}{2}\tau\right) e^{-\frac{\Omega_R}{2Q_R}\tau}, \quad (\text{A7a})$$

$$b(\tau) = \left\{ -\frac{\Gamma + 1}{\Omega_R} \sin\left(\frac{\Omega_R}{2}\tau\right) + \cos\left(\frac{\Omega_R}{2}\tau\right) \right\} e^{-\frac{\Omega_R}{2Q_R}\tau}, \quad (\text{A7b})$$

which are the sought-after amplitudes governing the time evolution of the coupled QE-cavity system [see Eqs. (7)].

-
- [1] P. Törmä and W. L. Barnes, *Rep. Prog. Phys.* **78**, 013901 (2015).
- [2] P. Vasa and C. Lienau, *ACS Photonics* **5**, 2 (2018).
- [3] C. Tserkezis, A. I. Fernández-Domínguez, P. A. D. Gonçalves, F. Todisco, J. D. Cox, K. Busch, N. Stenger, S. I. Bozhevolnyi, N. A. Mortensen, and C. Wolff, *Rep. Prog. Phys.* **83**, 082401 (2020).
- [4] J. Sun, Y. Li, H. Hu, W. Chen, D. Zheng, S. Zhang, and H. Xu, *Nanoscale* **13**, 4408 (2021).
- [5] X. Xiong, N. Kongsuwan, Y. Lai, C. E. Png, L. Wu, and O. Hess, *Appl. Phys. Lett.* **118**, 130501 (2021).
- [6] P. Dombi, Z. Pápa, J. Vogelsang, S. V. Yalunin, M. Siviš, G. Herink, S. Schäfer, P. Groß, C. Ropers, and C. Lienau, *Rev. Mod. Phys.* **92**, 025003 (2020).
- [7] A. I. Fernández-Domínguez, S. I. Bozhevolnyi, and N. A. Mortensen, *ACS Photonics* **5**, 3447 (2018).
- [8] E. M. Purcell, *Phys. Rev.* **68**, 681 (1946).
- [9] H. Walther, B. T. H. Varcoe, B.-G. Englert, and T. Becker, *Rep. Prog. Phys.* **69**, 1325 (2006).
- [10] A. F. Kockum, A. Miranowicz, S. De Liberato, S. Savasta, and F. Nori, *Nat. Rev. Phys.* **1**, 19 (2019).
- [11] S. Haroche and D. Kleppner, *Phys. Today* **42**(1), 24 (1989).
- [12] C. Weisbuch, M. Nishioka, A. Ishikawa, and Y. Arakawa, *Phys. Rev. Lett.* **69**, 3314 (1992).
- [13] T. Yoshie, A. Scherer, J. Hendrickson, G. Khitrova, H. M. Gibbs, G. Rupper, C. Ell, O. B. Shchekin, and D. G. Deppe, *Nature (London)* **432**, 200 (2004).
- [14] P. A. D. Gonçalves, N. Stenger, J. D. Cox, N. A. Mortensen, and S. Xiao, *Adv. Opt. Mater.* **8**, 1901473 (2020).
- [15] J. Bellessa, C. Bonnand, J. C. Plenet, and J. Mugnier, *Phys. Rev. Lett.* **93**, 036404 (2004).
- [16] J. Dintinger, S. Klein, F. Bustos, W. L. Barnes, and T. W. Ebbesen, *Phys. Rev. B* **71**, 035424 (2005).
- [17] G. Zengin, M. Wersäll, S. Nilsson, T. J. Antosiewicz, M. Käll, and T. Shegai, *Phys. Rev. Lett.* **114**, 157401 (2015).
- [18] Y. Sugawara, T. A. Kelf, J. J. Baumberg, M. E. Abdelsalam, and P. N. Bartlett, *Phys. Rev. Lett.* **97**, 266808 (2006).
- [19] R. Chikkaraddy, B. de Nijs, F. Benz, S. J. Barrow, O. A. Scherman, E. Rosta, A. Demetriadou, P. Fox, O. Hess, and J. J. Baumberg, *Nature (London)* **535**, 127 (2016).
- [20] K. Santhosh, O. Bitton, L. Chuntonov, and G. Haran, *Nat. Commun.* **7**, 11823 (2016).
- [21] C. Tserkezis, P. A. D. Gonçalves, C. Wolff, F. Todisco, K. Busch, and N. A. Mortensen, *Phys. Rev. B* **98**, 155439 (2018).
- [22] F. Todisco, R. Malureanu, C. Wolff, P. A. D. Gonçalves, A. S. Roberts, N. A. Mortensen, and C. Tserkezis, *Nanophotonics* **9**, 803 (2020).
- [23] G. W. Castellanos, S. Murai, T. V. Raziman, S. Wang, M. Ramezani, A. G. Curto, and J. Gómez Rivas, *ACS Photonics* **7**, 1226 (2020).
- [24] S. Shen, Y. Wu, Y. Li, P. Xie, Q. Ding, X. Kuang, W. Wang, and W. Wang, *Phys. Rev. B* **105**, 155403 (2022).
- [25] B. Gurlek, V. Sandoghdar, and D. Martín-Cano, *ACS Photonics* **5**, 456 (2018).
- [26] P. E. Stamatopoulou, V. Yannopapas, N. A. Mortensen, and C. Tserkezis, *Phys. Rev. B* **102**, 195415 (2020).
- [27] P. E. Stamatopoulou, S. Droulias, G. P. Acuna, N. A. Mortensen, and C. Tserkezis, *Nanoscale* **14**, 17581 (2022).
- [28] F. J. García-Vidal, C. Ciuti, and T. W. Ebbesen, *Science* **373**, eabd0336 (2021).
- [29] C. M. Bender, *Rep. Prog. Phys.* **70**, 947 (2007).
- [30] R. El-Ganainy, K. G. Makris, M. Khajavikhan, Z. H. Musslimani, S. Rotter, and D. N. Christodoulides, *Nat. Phys.* **14**, 11 (2018).
- [31] C. M. Bender and S. Boettcher, *Phys. Rev. Lett.* **80**, 5243 (1998).
- [32] K. G. Makris, R. El-Ganainy, D. N. Christodoulides, and Z. H. Musslimani, *Phys. Rev. Lett.* **100**, 103904 (2008).
- [33] A. Guo, G. J. Salamo, D. Duchesne, R. Morandotti, M. Volatier-Ravat, V. Aimez, G. A. Siviloglou, and D. N. Christodoulides, *Phys. Rev. Lett.* **103**, 093902 (2009).
- [34] H. Ramezani, T. Kottos, R. El-Ganainy, and D. N. Christodoulides, *Phys. Rev. A* **82**, 043803 (2010).
- [35] L. Feng, Y.-L. Xu, W. S. Fegadolli, M.-H. Lu, J. E. B. Oliveira, V. R. Almeida, Y.-F. Chen, and A. Scherer, *Nat. Mater.* **12**, 108 (2013).
- [36] B. Peng, Ş. K. Özdemir, F. Lei, F. Monifi, M. Gianfreda, G. L. Long, S. Fan, F. Nori, C. M. Bender, and L. Yang, *Nat. Phys.* **10**, 394 (2014).
- [37] Y. Huang, G. Veronis, and C. Min, *Opt. Express* **23**, 29882 (2015).
- [38] Z. Lin, H. Ramezani, T. Eichelkraut, T. Kottos, H. Cao, and D. N. Christodoulides, *Phys. Rev. Lett.* **106**, 213901 (2011).
- [39] D. L. Sounas, R. Fleury, and A. Alù, *Phys. Rev. Appl.* **4**, 014005 (2015).
- [40] L. Feng, Z. J. Wong, R.-M. Ma, Y. Wang, and X. Zhang, *Science* **346**, 972 (2014).
- [41] H. Hodaie, M.-A. Miri, M. Heinrich, D. N. Christodoulides, and M. Khajavikhan, *Science* **346**, 975 (2014).
- [42] Z. Gao, S. T. M. Fryslie, B. J. Thompson, P. S. Carney, and K. D. Choquette, *Optica* **4**, 323 (2017).
- [43] M. P. Hokmabadi, A. Schumer, D. N. Christodoulides, and M. Khajavikhan, *Nature (London)* **576**, 70 (2019).

- [44] S. Sanders and A. Manjavacas, *Nanophotonics* **9**, 473 (2020).
- [45] J. Wiersig, *Phys. Rev. Lett.* **112**, 203901 (2014).
- [46] H. Hodaie, A. U. Hassan, S. Wittek, H. Garcia-Gracia, R. El-Ganainy, D. N. Christodoulides, and M. Khajavikhan, *Nature (London)* **548**, 187 (2017).
- [47] W. Chen, Ş. K. Özdemir, G. Zhao, J. Wiersig, and L. Yang, *Nature (London)* **548**, 192 (2017).
- [48] N. A. Mortensen, P. A. D. Gonçalves, M. Khajavikhan, D. N. Christodoulides, C. Tserkezis, and C. Wolff, *Optica* **5**, 1342 (2018).
- [49] J. Wiersig, *Photonics Res.* **8**, 1457 (2020).
- [50] S. N. Ghosh and Y. D. Chong, *Sci. Rep.* **6**, 19837 (2016).
- [51] A. V. Sadovnikov, A. A. Zyablovsky, A. V. Dorofeenko, and S. A. Nikitov, *Phys. Rev. Appl.* **18**, 024073 (2022).
- [52] V. M. Agranovich, M. Litinskaia, and D. G. Lidzey, *Phys. Rev. B* **67**, 085311 (2003).
- [53] S. Franke, J. Ren, and S. Hughes, *Phys. Rev. A* **105**, 023702 (2022).
- [54] S. Fan, W. Suh, and J. D. Joannopoulos, *J. Opt. Soc. Am. A* **20**, 569 (2003).
- [55] Excitons, being quasiparticles made of two elementary fermions, are often well-described as *composite bosons* [56] and thus exhibiting bosonic character (bosonic commutation relations [57], Bose-Einstein condensation [58], etc.) in the low-density limit. In some circumstances, however, they can behave more like fermions or even exhibit mixed bosonic and fermionic effects [59,60].
- [56] M. Combescot and S.-Y. Shiao, *Excitons and Cooper Pairs: Two Composite Bosons in Many-Body Physics* (Oxford University Press, New York, 2015).
- [57] F. Katsch, M. Selig, A. Carmele, and A. Knorr, *Phys. Stat. Sol. (b)* **255**, 1800185 (2018).
- [58] V. M. Pereira, *Nat. Phys.* **18**, 6 (2021).
- [59] M. Combescot, M. Betbeder-Matibet, and F. Dubin, *Phys. Rep.* **463**, 215 (2008).
- [60] M. Katzer, M. Selig, L. Sigl, M. Troue, J. Figueiredo, J. Kiemle, F. Sigger, U. Wurstbauer, A. W. Holleitner, and A. Knorr, *arXiv:2303.11787* (2023).
- [61] Y. Li, X. Ma, Z. Hatzopoulos, P. G. Savvidis, S. Schumacher, and T. Gao, *ACS Photonics* **9**, 2079 (2022).
- [62] J. J. Geuchies, B. Brynjarsson, G. Grimaldi, S. Gudjonsdottir, W. van der Stam, W. H. Evers, and A. J. Houtepen, *ACS Nano* **15**, 377 (2021).
- [63] S. Morozov, C. Wolff, and N. A. Mortensen, *Adv. Opt. Mater.* **9**, 2101305 (2021).
- [64] R. C. Keitel, M. Aellen, B. le Feber, A. A. Rossinelli, S. A. Meyer, J. Cui, and D. J. Norris, *Nano Lett.* **21**, 8952 (2021).
- [65] R. R. Cooney, S. L. Sewall, D. M. Sagar, and P. Kambhampati, *Phys. Rev. Lett.* **102**, 127404 (2009).
- [66] I. B. Martini, I. M. Craig, W. C. Molenkamp, H. Miyata, S. H. Tolbert, and B. J. Schwartz, *Nat. Nanotechnol.* **2**, 647 (2007).
- [67] M. Wersäll, J. Cuadra, T. J. Antosiewicz, S. Balci, and T. Shegai, *Nano Lett.* **17**, 551 (2017).
- [68] F. Todisco, M. De Giorgi, M. Esposito, L. De Marco, A. Zizzari, M. Bianco, L. Dominici, D. Ballarini, V. Arima, G. Gigli, and D. Sanvitto, *ACS Photonics* **5**, 143 (2018).
- [69] M. Geisler, X. Cui, J. Wang, T. Rindzevicius, L. Gammelgaard, B. S. Jessen, P. A. D. Gonçalves, F. Todisco, P. Bøggild, A. Boisen, M. Wubs, N. A. Mortensen, S. Xiao, and N. Stenger, *ACS Photonics* **6**, 994 (2019).
- [70] Z.-J. Yang, T. J. Antosiewicz, and T. Shegai, *Opt. Express* **24**, 20373 (2016).
- [71] A. Maity, S. Maithani, and M. Pradhan, *Anal. Chem.* **93**, 388 (2021).
- [72] N. W. Ashcroft and N. D. Mermin, *Solid State Physics* (Harcourt, Orlando, FL, 1976).
- [73] M. Stührenberg, B. Munkhbat, D. G. Baranov, J. Cuadra, A. B. Yankovich, T. J. Antosiewicz, E. Olsson, and T. Shegai, *Nano Lett.* **18**, 5938 (2018).
- [74] P. Bouteyre, H. S. Nguyen, J.-S. Lauret, G. Trippé-Allard, G. Delport, F. Lédée, H. Diab, A. Belarouci, C. Seassal, D. Garrot, F. Bretenaker, and E. Deleporte, *ACS Photonics* **6**, 1804 (2019).
- [75] D. G. Lidzey, D. D. C. Bradley, M. S. Skolnick, T. Virgili, S. Walker, and D. M. Whittaker, *Nature (London)* **395**, 53 (1998).
- [76] P. Vasa, W. Wang, R. Pomraenke, M. Lammers, M. Maiuri, C. Manzoni, G. Cerullo, and C. Lienau, *Nat. Photonics* **7**, 128 (2013).
- [77] G. Scalari, C. Maissen, D. Turčinková, D. Hagenmüller, S. De Liberato, C. Ciuti, C. Reichl, D. Schuh, W. Wegscheider, M. Beck, and J. Faist, *Science* **335**, 1323 (2012).
- [78] D. Dini, R. Köhler, A. Tredicucci, G. Biasiol, and L. Sorba, *Phys. Rev. Lett.* **90**, 116401 (2003).
- [79] G. Rempe, F. Schmidt-Kaler, and H. Walther, *Phys. Rev. Lett.* **64**, 2783 (1990).
- [80] M. Brune, F. Schmidt-Kaler, A. Maali, J. Dreyer, E. Hagley, J. M. Raimond, and S. Haroche, *Phys. Rev. Lett.* **76**, 1800 (1996).
- [81] F. Brennecke, T. Donner, S. Ritter, T. Bourdel, M. Köhl, and T. Esslinger, *Nature (London)* **450**, 268 (2007).
- [82] L. Mao, C. C. Stoumpos, and M. G. Kanatzidis, *J. Am. Chem. Soc.* **141**, 1171 (2019).
- [83] R. Su, A. Fieramosca, Q. Zhang, H. S. Nguyen, E. Deleporte, Z. Chen, D. Sanvitto, T. C. H. Liew, and Q. Xiong, *Nat. Mater.* **20**, 1315 (2021).
- [84] M. O. Scully and M. S. Zubairy, *Quantum Optics* (Cambridge University Press, Cambridge, 1997).
- [85] G. S. Agarwal, *Quantum Optics* (Cambridge University Press, Cambridge, 2013).